Inorganic Chemistry

Article

pubs.acs.org/IC

Crystal and Magnetic Structures and Magnetic Properties of Selenate Containing Natrochalcite, $A^{I}M^{II}_{2}(H_3O_2)(SeO_4)_2$ Where A = Na or K and M = Mn, Co, or Ni

Wassim Maalej,[†,‡] Serge Vilminot,*[,†] Gilles André,[§] Zakaria Elaoud,[‡] Tahar Mhiri,[‡] and Mohamedally Kurmoo*[,∥]

[†]Département de Chimie des Matériaux Inorganiques, IPCMS, UMR 7504 (CNRS-UdS), 23 rue du Loess, BP 43, 67034 Strasbourg Cedex 02, France

[‡]Laboratoire de l'Etat Solide, Faculté des Sciences, Université Sfax, route de Skoura km 3,5, 3000 Sfax, Tunisia

[§]Laboratoire Léon Brillouin, CEA-CNRS, CEA Saclay, 91191 Gif-sur-Yvette, France

[∥]Laboratoire DECOMET, CNRS-UMR 7177, Institut de Chimie de Strasbourg, Université de Strasbourg, 4 rue Blaise Pascal, 67000 Strasbourg Cedex 1, France

Supporting Information

ABSTRACT: The synthesis of a series of selenate containing natrochalcite, $A^{I}M^{II}_{2}(H_3O_2)(SeO_4)_2$ where A = Na or K and M = Mn, Co, or Ni (here labeled as **AMH** and **AMD** for the hydrogenated and deuterated compounds, respectively), the X-ray crystal structure determinations from single crystals (Ni) and powder (Mn), magnetic properties, and magnetic structures of the cobalt analogues are reported. The nuclear crystal structures for **NaNiH**, **KNiH**, and **KMnH** are similar to those reported for the cobalt analogues (**NaCoH** and **KCoH**) and consist of chains of edge-sharing octahedra (MO_6) which are connected by H_3O_2 and SeO_4 to form layers which are in turn bridged by the alkali, in an octahedral coordination site, to form the 3D-framework. The magnetic properties are characterized by antiferromagnetic interaction at high temperatures and antiferromagnetic ordering at low temperatures (**NaCoH**, 3.5 K; **KCoH**, 5.9 K; **KNiH**, 8.5 K; and **KMnH**, 16 K), except for $KNi_2(H_3O_2)(SeO_4)_2$ which displays a weak ferromagnetic interaction and no long-range ordering above 2 K. The neutron magnetic structures of the cobalt analogues, studied as a function of temperature, are different for the two cobalt salts and also different from all the known magnetic structures of the natrochalcite family. Whereas the magnetic structure of **NaCoD** has a k = (0, 0, 0), that of **KCoD** has one consisting of a doubled nuclear cell, k = (0, 0, 1/2). Both compounds have four magnetic sublattices related to the four cobalt atoms of the nuclear unit cell. In **NaCoD** the moments are in the bc-plane, M_y = 2.51(2) μ_B and M_z = 1.29(4) μ_B, with the major component along the cobalt chain and the resultant moment, 2.83(3) μ_B, making an angle of 27° with the b-axis. The sum of the moments within the cell is zero. For **KCoD** the moment at each cobalt site has a component along each crystallographic axis, M_x = 2.40(3), M_y = 1.03(3), M_z = 1.59(8) giving a total M = 2.49(3) μ_B. Within one nuclear cell the moments are fully compensated. The moments corresponding to the cobalt atoms of the second nuclear cell comprising the magnetic unit cell are oriented in opposite directions.

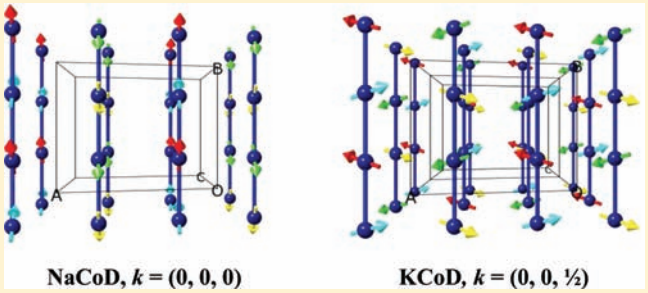

1. INTRODUCTION

The sequence of events in the study of magnetism and magnetic structures using neutron diffraction started with magnetic minerals and especially oxides of the general structural families, viz, rocksalt, spinel, rutile, and perovskite.[1] For these materials, the structures are composed of only polyhedra of magnetic ions.[2] The next sets of materials to be studied were those containing polyhedra of both magnetic and nonmagnetic ions and for the latter the natural salts contain sulfate, borate, phosphate and arsenate.[3] These were expanded synthetically with other ones, such as vanadate, selenate, and others.[3,4] Very few studies have been performed on sulfate until the rise of interest in understanding the frustration in magnetism, consequent to the presence of structural triangular motifs, where there were major developments on jarosites and kagome layered systems.[5]

The few magnetic structure studies on minerals containing octahedral magnetic transition metals and tetrahedral non-magnetic anions prompted us to study first Antlerite, a product of pollution, which gives the statue of liberty its green coloration, and its selenate analogue.[6,7] This led to the

Received: October 19, 2011
Published: January 20, 2012

   dx.doi.org/10.1021/ic202273e | Inorg. Chem. 2012, 51, 1953−1962

Table 1. Summary of Crystal and Magnetic Structures and Magnetic Properties of Some Natrochalcites[a]

compound	space group - crystal form	Θ/K	$T_{Néel}$ / K [canting angle/°]	k(x, y, z)	LRO	SRO	M_x / μ_B	M_y / μ_B	M_z / μ_B	ref
$NaCu_2(H_3O_2)(SO_4)_2$	$C2/m$ - SC	+9.9	3.3							13
$NaNi_2(H_3O_2)(MoO_4)_2$	$C2/m$ - P	−12.9(3)	28 [0.30]	0, 0, 0	yes	yes	0.5(1)	0	1.65(6)	14a
$NaCo_2(H_3O_2)(MoO_4)_2$	$C2/m$ - SC	−47(1)	21 [0.17]	0, 0, 0	yes	yes	0	2.95(2)	0	14a
$NaFe_2(H_3O_2)(MoO_4)_2$	$C2/m$ - SC	−24.7(3)	17	0, 0, 0	yes	no	3.09(3)	0	0.41(3)	14c
				0, 0, 1/2			0.83(2)	2.48(4)	0	
$KCo_2(H_3O_2)(MoO_4)_2$	$I2/m$ - P	−17.1(3)								14b
$KFe_2(H_3O_2)(MoO_4)_2$	$I2/m$ - P		11	1/2, 0, 1/2	yes	no	0	3.55(3)	0	14b
$KMn_2(H_3O_2)(MoO_4)_2$	$I2/m$ - P	−52.6(2)	8.2	1/2, 0, 1/2	yes	yes	3.90(3)	0	1.57(9)	14b
$NaCo_2(H_3O_2)(SeO_4)_2$	$C2/m$ - SC	−15.5(3)	3.5	0, 0, 0	yes	yes	0	2.51(2)	1.29(4)	this work
$NaNi_2(H_3O_2)(SeO_4)_2$	$C2/m$ - SC	+1.5(2)								this work
$KCo_2(H_3O_2)(SeO_4)_2$	$C2/m$ - SC	−26.1(6)	5.9	0, 0, 1/2	yes	no	2.40(3)	1.03(3)	1.59(8)	this work
$KNi_2(H_3O_2)(SeO_4)_2$	$C2/m$ - SC	−11.2(4)	8.5							this work
$KMn_2(H_3O_2)(SeO_4)_2$	$C2/m$ - P	−30.9(7)	16							this work

[a] Θ = Weiss constant; k(x, y, z) = propagation magnetic vector; LRO = long-range magnetic ordering; SRO = short-range magnetic ordering; M_i = magnetic moment along the i-axis obtained from neutron diffraction; SC = single crystal; P = powder.

observation that Antlerite has a simple magnetic structure (k = 0, 0, 0), but with an idle moment on the central copper of the trimer within the structure. In contrast, the selenate analogue displays a very unusual and rarely observed cycloidal magnetic structure becoming commensurate at the lowest temperatures with a vector $k = k_x$, 0, 0 where $k_x = 1/7$.[7] This work then followed those of the antiferromagnet brochantite $[Cu_4(OH)_6(SO_4)]$,[8] the ferrimagnet lindgrenite $[Cu_3(OH)_2(MoO_4)_2]$[9] and three sets of synthetic compounds, $M_3(OH)_2(SO_4)_2(H_2O)_2$,[10] $K_2M_3(OH)_2(SO4)_3(H_2O)_2$,[11] and $Co_5(OH)_6(TO_4)_2(H_2O)_4$[12] where M = Mn, Fe, Co, Ni and T = S or Se. The first of these sets are canted antiferromagnets, the second are ferrimagnets, and the last are ferromagnets. The last family of compounds that we are studying is that of natrochalcite, $AM_2(H_3O_2)(TO_4)_2$.[13,14]

The synthesis and crystal chemistry using X-ray, and in some cases neutron diffraction, of the mineral natrochalcite, $AM_2(H_3O_2)(TO_4)_2$, family are well documented,[13−20] but their magnetic properties and magnetic structures remained unknown until the reported antiferromagnetism of $NaCu_2(D_3O_2)(SO_4)_2$ (T_N = 3.3 K) and $NaM_2(H_3O_2)(MoO_4)_2$ (M = Ni (T_N = 21 K) and Co (T_N = 28 K)).[13,14] Previous works were concerned principally with the syntheses, characterization, and identification of the geometry and function of the H_3O_2 anion. It has been demonstrated that a wide range of salts can be prepared with A of varying sizes (Na, K, Cs, Rb, Tl, NH_4, and Ag), M of the divalent transition metals (Mn, Fe, Co, Ni, Cu, and Zn), and the central atom of the tetrahedral anion (T) being S, Se, or Mo.[13−20] Although the known salts contain principally divalent metals, one has been reported to contain trivalent iron. Such a variety of possible cations (A, M, and T) in the three crystallographic sites provide a handful of materials for systematically studying their influence on the magnetic properties and magnetic structures as a function of cationic sizes, spin, and magnetic anisotropy.[14,20]

Previous work on the molybdate family and the present one on the selenate family indicate that all display long-range antiferromagnetic ordering with the exception of a couple (Table 1).[13,14] The exceptions do not show any long-range ordering at temperatures above 2 K. In another couple of cases canting of the moments were detected in the magnetic properties. The Néel transition temperatures vary widely and unsystematically. Most surprising is the variety and unpredictable magnetic structures that have been observed and the unprecedented observation of two concomitant magnetic structures for the 2D-Ising antiferromagnet, $NaFe_2(D_3O_2)(MoO_4)_2$.[14c] The present study was undertaken in search of clues to the unexpected inconsistencies in the magnetic properties and magnetic structures.

Here, we present the crystal structures of three unknown ones, two from single crystal data (**NaNiH** and **KNiH**) and one from powder data (**KMnH**), the magnetic properties as a function of temperature and field, and the magnetic structures of the two cobalt analogues (**NaCoD** and **KCoD**) for which deuterated samples were obtained in the required quantity. With the exception of **KNiH** all the compounds exhibit long-range magnetic ordering above 2 K. The two cobalt compounds have magnetic structures belonging to two different propagation vectors, k = (0, 0, 0) for **NaCoD** and k = (0, 0, 1/2) for **KCoD**.

2. EXPERIMENTAL SECTION

Synthesis. All the compounds were prepared by hydrothermal technique using a fill factor of 1/3 of the 125-mL capacity Teflon-lined stainless steel autoclaves. As the transition metal selenates are not available commercially, we have prepared them by the reaction of $MnCO_3·4H_2O$, $CoCO_3·4H_2O$, or $NiCO_3·2Ni(OH)_2$ with an excess of selenic acid (H_2SeO_4, 40 wt % water solution). When the resulting solutions were slowly evaporated at room temperature $MnSeO_4·2H_2O$, $CoSeO_4·4H_2O$, or $NiSeO_4·6H_2O$ were obtained. If the solutions were kept at 60 °C the monohydrated salts, $MSeO_4·H_2O$, were obtained. The formulas and

dx.doi.org/10.1021/ic202273e | Inorg. Chem. 2012, 51, 1953−1962

Table 2. Summary of the Single-Crystal X-ray Data for NaNiH and KNiH

	NaNiH	KNiH
formula	$Se_2H_3NaO_{10}Ni_2$	$Se_2H_3KO_{10}Ni_2$
	$NaNi_2(H_3O_2)(SeO_4)_2$	$KNi_2(H_3O_2)(SeO_4)_2$
formula weight	461.31	477.42
temperature (K)	173	173
a (Å)	8.8476(4)	8.9687(3)
b (Å)	6.2451(3)	6.3505(2)
c (Å)	7.4883(4)	7.6587(2)
β (°)	114.531(1)	113.382(1)
V (Å^3)	376.41(3)	411.73(2)
Z	2	2
system	monoclinic	monoclinic
space group	$C2/m$	$C2/m$
F (000)	436	452
D_{calcd} (g·cm^{-3})	4.07	3.85
radiation, λ (Å)	Mo Kα_1, 0.71069	Mo Kα_1, 0.71069
μ (mm^{-1})	1.48	1.396
hkl range	$-11 < h < 10$, $-4 < k < 8$, $-9 < l < 9$	$-11 < h < 11$, $-8 < k < 8$, $-9 < l < 9$
θ range (°)	4.13−27.46	2.90−27.42
measured reflections	1276	4614
unique reflections	460	498
unique $I > 2\sigma(I)$	452	485
R_{int} (%)	0.0135	0.0177
R1 (all data) (%)	0.0145	0.0117
wR2(F_o2) (all data) (%)	0.0404	0.0301
GoF (%)	1.176	1.009
residual electron density	−0.451/+0.536	−0.336/+0.286

compositions were checked by powder X-ray diffraction and TGA analyses.

For $KCo_2(H_3O_2)(SeO_4)_2$ (**KCoH**), $CoSeO_4{\cdot}4H_2O$ (2.5 g, 9.1 mmol) was dissolved in 20 mL of boiled distilled water, and KOH (0.39 g, 5.9 mmol) and K_2SeO_4 (0.65 g, 2.9 mmol) were dissolved in 20 mL of boiled distilled water. The resulting solutions were mixed under stirring giving rise to a blue suspension, which was poured into the PTFE-lined stainless steel pressure vessel and heated at 200 °C for 2 days. The resulting pink polycrystalline powder was retrieved by filtration, washed with water, alcohol, and acetone before drying at 40 °C. Yield = 85%.

$KCo_2(D_3O_2)(SeO_4)_2$ (**KCoD**) was obtained using a similar procedure but using heavy water (D_2O) instead. Elemental analyses: % found (% calculated); Co 25.6 (24.7); Se 33.0 (33.0); K 7.6 (8.2).

For $NaCo_2(H_3O_2)(SeO_4)_2$ (**NaCoH**), $CoSeO_4{\cdot}H_2O$ (1 g, 4.5 mmol) was dissolved in 20 mL of boiled distilled water, and NaOH (0.12 g, 3 mmol) was dissolved in 20 mL of boiled distilled water. The resulting solutions were mixed under stirring giving rise to a blue suspension, which was poured into the PTFE-lined stainless steel pressure vessel and heated at 200 °C for 2 days. The resultant pink polycrystalline powder was retrieved by filtration, washed with water, alcohol, and acetone before drying at 40 °C. Yield = 80%.

$NaCo_2(D_3O_2)(SeO_4)_2$ (**NaCoD**) was obtained using a similar procedure but using heavy water (D_2O) instead. Elemental analyses: % found (% calculated); Co 25.8 (25.5); Se 34.2 (34.2); Na 4.8 (5.0).

$NaNi_2(H_3O_2)(SeO_4)_2$ (**NaNiH**) was prepared as for **NaCoH** starting from $NiSeO_4{\cdot}6H_2O$ (1 g, 3.2 mmol), NaOH (0.06 g, 1.5 mmol), and a temperature of 240 °C for 4 days. Green block crystals were harvested in 35% yield.

For $KNi_2(H_3O_2)(SeO_4)_2$ (**KNiH**), a procedure similar to that for **KCoH** starting from $NiSeO_4{\cdot}6H_2O$ (1.36 g, 4.4 mmol), KOH (0.29 g, 4.4 mmol), K_2SeO_4 (0.32 g, 1.5 mmol), and using a temperature of 240 °C for 4 days gave green crystals which were collected by decantation, washed with water, ethanol, and acetone, and dried in air. The yield was 27%.

For $KMn_2(H_3O_2)(SeO_4)_2$ (**KMnH**), a procedure similar to that for **KCoH** starting from $MnSeO_4{\cdot}2H_2O$ (1 g, 4.3 mmol), KOH (0.17 g, 2.6 mmol), K_2SeO_4 (1.88 g, 8.5 mmol), a mixture of 1:1 water ethanol instead of pure water, and using a temperature of 170 °C for 2 days gave a yellow powder which was collected by filtration, washed with water, ethanol, and acetone, and dried in air. The yield was 15%.

Only **KCoD** and **NaCoD** were obtained in sufficient quantities for neutron experiments.

Characterizations. Infrared spectra were recorded by transmission through KBr pellets containing 1% of the crystals using a Digilab Excalibur Series FTIR spectrometer. TG-DTA analyses were performed on a TA-SDT-Q600 apparatus under air or argon at a heating rate of 5 °C/min in a platinum crucible. Powder X-ray diffraction patterns were recorded using a D8 Bruker diffractometer (Cu Kα_1, 1.5406 Å), equipped with a front monochromator. EDX analyses were made using a Kevex unit of a Jeol 6700 F SEM apparatus. Elemental analyses were performed by ICP method on the deuterated cobalt samples, **NaCoD** and **KCoD**, in order to check their purity before neutron diffraction experiments. Magnetization measurements were performed in the temperature range 2−300 K and field up to 50 kOe by means of a Quantum Design MPMS-XL SQUID magnetometer. More specific details are given in the text.

X-ray Crystal Structure Determinations. Single crystal X-ray diffraction data were collected on a Nonius Kappa CCD

dx.doi.org/10.1021/ic202273e | Inorg. Chem. 2012, 51, 1953−1962

diffractometer using monochromatized Mo $K\alpha_1$ radiation. Block crystals of **NaNiH** and **KNiH** were mounted on glass fibers and cooled by a N_2 stream for data collection at 173 K. The structures were solved by direct methods with SHELXS-97 and refined using SHELXL-97.[21] The final refinements included anisotropic displacement parameters for all non-hydrogen atoms and isotropic ones for hydrogen atoms. Additional details are given in Table 2. Tables S1 and S2 give the final atomic positions and Table 3 gives the corresponding bond lengths and angles. Further details of the crystal structure investigation may be obtained from the CIF files, which have been deposited at the Fachinformationzentrum Karlsruhe, 76344 Eggenstein-Leopoldshafen, Germany, on quoting the depository number CSD-422960 and 422961 (it can be requested from Crysdata@FIZ-Karlsruhe.de).

Neutron Magnetic Structure Determinations. The neutron diffraction experiments were performed at the Laboratoire Léon Brillouin (CEA Saclay) using the multi-detector (800 cells) G4.1 (λ = 2.4266 Å) diffractometer for the determination of the magnetic structure and the thermal evolution study of the low temperature patterns. Eleven and nine diffraction patterns were recorded in the 2θ ranges 8°−87.9° and 6°−85.9° for **NaCoD** and **KCoD**, respectively, at different temperatures between 1.7 and 8 K. The powder samples were packed in cylindrical vanadium cans and held in a liquid helium cryostat. Nuclear and magnetic structures were refined using the FULLPROF program.[22] The nuclear scattering lengths (b_{Na} = 0.3630 × 10^{-12} cm, b_K = 0.3670 × 10^{-12} cm, b_{Co} = 0.2490 × 10^{-12} cm, b_{Se} = 0.7070 × 10^{-12} cm, b_O = 0.5803 × 10^{-12} cm, b_D = 0.6671 × 10^{-12} cm, b_H = −0.3739 × 10^{-12} cm) and Co(II) magnetic form factors were those included in this program.

3. RESULTS AND DISCUSSION

Synthesis. Different parameters such as concentration, pH, filling factor, time, and temperature have been varied to obtain single phase of the aimed compounds (Figure S1), and improve on their purity, their crystallinity, and the yields of the reactions. The temperature varies according to the compound going from 170 °C for **KMnH** to 200 °C for the cobalt compounds and 240 °C for the nickel ones. The optimized temperature of the reaction for each metal ion follows the same trend as the decomposition temperature found in the thermogravimetry measurements (see later). Whereas only powders were obtained for Mn and Co compounds, single crystals of dimensions suitable for X-ray diffraction measurements were obtained for **NaNiH** and **KNiH**. For Mn, a mixture of water and ethanol was required; the presence of ethanol promoting a higher pressure that probably favors the reaction. The yields depended on the transition metal with high value for Co (∼80%) and low ones for Mn (15%) and Ni (∼30%). Therefore, the syntheses using D_2O for neutron powder diffraction measurements were restricted to the cobalt compounds. The color of the compounds varied from yellow for Mn to pink for Co and green for Ni. Finally, it has to be noted that all attempts to make **NaMnH** have been unsuccessful. This compound combines the smaller alkali ion with the biggest metal (Mn) and this incompatibility could be responsible for the fact that **NaMnH** is not obtained. This is also observed for the molybdate series.[14]

Powder X-ray Diffraction. The X-ray powder patterns (Figure 1) of the basic selenates are quite similar and differ by 2θ shifts of the lines in agreement with the modification of the unit cell parameters according to the nature of the metal ions. By means of the DICVOL and FULLPROF programs, the unit cell parameters have been refined and are given in Table S3.[22,23]

The powder diffraction patterns have all been indexed in the space group $C2/m$ with parameters of natrochalcite-type structure. The patterns were fitted using the leBail pattern matching routine to refine the unit cell parameters (Figures S2−S6 and Table S3). It is to be noted the presence of some

Table 3. Bond Distances (Å) and Angles (°) for NaNiH and KNiH

compound	NaNiH	KNiH
	Ni environment	
Ni−OH x2	2.0042(12)	2.0641(10)
Ni−O3 x2	2.0742(15)	2.0400(11)
Ni−O2 x2	2.1061(13)	2.1782(11)
<Ni−O>	2.0615	2.0941
OH-Ni−OH	180.0	180.0
OH−Ni-O3 x2	89.47(7)	88.06(6)
OH−Ni-O3 x2	90.53(7)	91.94(6)
OH−Ni-O2 x2	79.99(6)	77.56(5)
OH−Ni-O2 x2	100.01(6)	102.44(5)
O3−Ni−O3	180.0	180.0
O3−Ni−O2 x2	88.95(7)	89.01(5)
O3−Ni−O2 x2	91.05(7)	90.99(5)
O2−Ni−O2	180.0	180.0
	Se environment	
Se−O1	1.613(2)	1.6091(17)
Se−O2	1.6718(19)	1.6790(16)
Se−O3 x2	1.6430(14)	1.6736(12)
<Se−O>	1.643	1.6588
O1−Se−O2	106.41(11)	109.05(9)
O1−Se−O3 x2	111.37(7)	110.15(5)
O2−Se−O3 x2	108.69(6)	107.34(5)
O3−Se−O3	110.18(10)	112.67(8)
	Na/K environment	
Na/K−O1 x2	2.424(2)	2.7230(19)
Na/K−O2 x2	2.974(2)	2.9788(16)
Na/K−O3 x4	2.5183(15)	2.7396(12)
<Na/K−O>		
6-fold	2.487	2.7341
8-fold	2.609	2.7953
O1−Na/K-O1	180.0	180.0
O1−Na/K-O3 x4	76.81(5)	78.38(4)
O1−Na/K-O3 x4	103.19(5)	101.62(4)
O3−Na/K-O3 x2	90.35(7)	93.78(5)
O3−Na/K-O3 x2	89.65(7)	86.22(5)
O3−Na/K-O3 x2	180.0	180.0
	hydrogen bonding	
H1-OH	0.76(5)	0.76(4)
H1...O1	2.02(5)	2.18(4)
H2-OH	0.79(7)	0.77(7)
H2-OH′	1.66(7)	1.71(7)
OH...OH′	2.445(2)	2.487(2)
H1−H2	1.25(8)	1.26(8)
H1−H2′	2.10(8)	2.12(8)
H2−H2′	0.89(10)	0.94(10)
OH-H1...O1	179(4)	171(3)
OH-H2-OH′	173(6)	179(6)
H1-OH-H2	109(12)	111(12)
H1-OH-H2′	116(9)	112(8)

dx.doi.org/10.1021/ic202273e | Inorg. Chem. 2012, 51, 1953−1962

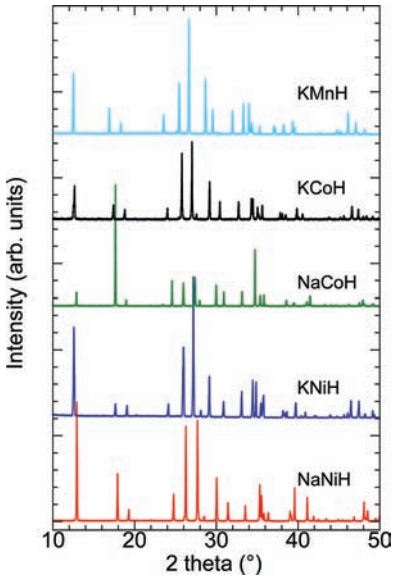

Figure 1. Powder X-ray diffraction patterns (Cu Kα_1) of the basic selenates (see LeBail pattern matching fits for each pattern in Figures S2–S6).

preferential orientations. As expected, the *a*, *b*, *c*, and *V* parameters increase from Ni to Mn in agreement with the evolution of the corresponding ionic radii, 0.70, 0.735, and 0.82 Å for Ni, Co, and Mn, respectively.[24] For a given transition metal, a similar evolution is observed from Na (1.02 Å) to K (1.38 Å), ionic radii for 6-fold environment.

Crystal Structure. Table 2 summarizes the crystal data and details of the refinements, Table 3 gives the interatomic bond lengths and angles and Tables S1 and S2 provide the atomic positions for the two nickel compounds. The structures consist of chains of edge-shared NiO_6 octahedra running along the *b*-axis direction (Figure 2). The NiO_6 octahedron is quite regular with <Ni–O> distances of 2.062/2.094 Å for Na/K and angles that deviate from 0.6/1.1% to 11.1/13.8% from the expected 90° value. The chains are connected by three kinds of three-atom bridges involving H_3O_2, SeO_4, giving rise to layers parallel to *ab* and Na/KO_6 connecting the layers in a 3D network (Figure 2). The SeO_4 tetrahedron is slightly distorted with Se–O distances (1.643/1.659 Å) very close to the ones observed in the corresponding Co compounds (1.644/1.644 Å).[18] Two O3 oxygen atoms are bonded to two neighboring octahedra, O2 is bridging two octahedra of another chain, and O1 is terminal. Therefore, each octahedron shares four corners with four SeO_4 tetrahedra.

The Na/KO_6 octahedron is distorted with Na/K–O bond lengths slightly shorter than those for the corresponding Co samples. For Na, the mean bond length for 6-fold coordination (2.487 Å) is bigger than the sum of the ionic radii (2.40 Å).[24] The same result is true when considering 8-fold coordination, 2.609 and 2.55 Å, respectively. On the other hand, the mean K–O distance is close to the sum of the ionic radii for 6-fold and smaller than for 8-fold coordination. If one considers the bond valence sums, values of 0.951 (6-fold) and 1.035 (8-fold) are observed for Na, evidencing a 6 + 2 coordination, whereas for K the value for 6-fold, 1.256, is much closer to 1 than for 8-fold, 1.459, octahedral environment appearing more realistic for this ion.[25]

The coordinating oxygen atoms of the three groups, OH, H_2O, and SeO_4, are of three types, μ_2 for OH and O1, μ_3 for O3, and μ_4 for O2. Concerning the H_3O_2 group, refinements involving either a split position around a center of symmetry for the H2 atom or H2 located on this center of symmetry yield very similar results as far as merit factors are concerned. Whatever the position of the H2 atom, the hydrogen bond through this atom is strong since the OH···OH distance is 2.445(2)/2.487(2) Å, i.e., much shorter than the sum of the van der Waals radii, 3.04 Å. The H–O–H···OH′ hydrogen bond is nearly linear with an angle of 173/179° as expected for this type.[26]

The structure determination of **KMnH** from powder data gives similar results (Tables S3 and S4 and Figure S7).

Thermal Analyses. The TGA traces of all the samples under air reveal the presence of a first weight loss between 230 and 540 °C according to the nature of the transition metal cations, associated with an endotherm having its maximum between 325 and 520 °C. This has been attributed to the departure of 1.5 water molecule, as shown in Table S5. A second weight loss takes place between 390 and 635 °C and is related to the decomposition of the selenate group as SeO_3. A final weight loss is evidenced for Co (905 °C) compounds corresponding to the reduction of Co_3O_4 formed during the decomposition process. The total weight loss agrees with the values calculated assuming the presence of a mixture containing $0.5A_2SeO_4$ and 2MO (Mn_2O_3 for Mn). XRD patterns recorded

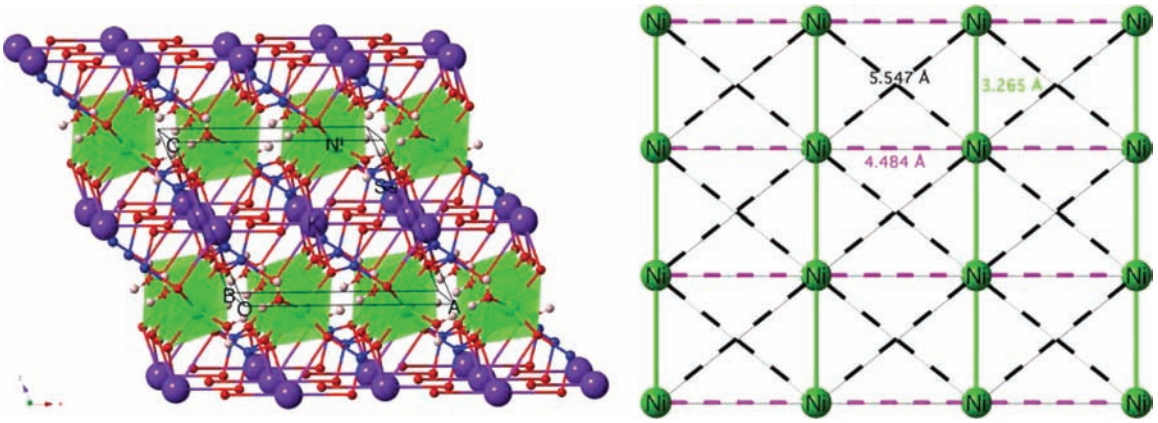

Figure 2. Projection of the structure of **KNiH** on the *ac*-plane (left). NiO_6 (green polyhedra), K (purple), O (red), Se (blue), H (pink), and the different magnetic exchange pathways within a layer in the *ab*-plane (right).

dx.doi.org/10.1021/ic202273e | *Inorg. Chem.* 2012, 51, 1953–1962

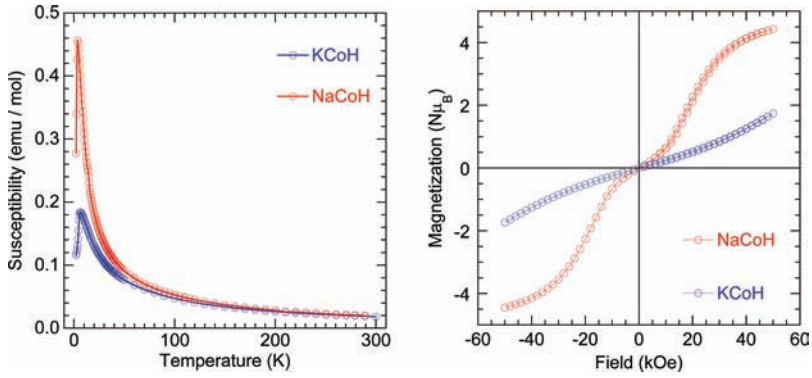

Figure 3. (a) Temperature dependence of the DC magnetic susceptibility of **NaCoH** and **KCoH** on cooling in a field of 100 Oe. (b) Isothermal magnetization at 2 K for **NaCoH** and **KCoH**.

Table 4. Magnetic Data for the Basic Selenates

compound	C (emu K/mol)	θ (K)	g	μ_{eff} (emu K/mol)	T_N (K)
NaNiH	2.64(1)	+1.5(2)	2.30	3.25	
KNiH	2.72(1)	−11.2(4)	2.33	3.30	8.5
NaCoH	6.11(1)	−14.7(5)	2.55	4.95	3.5
KCoH	5.99(2)	−27(1)	2.52	4.89	5.9
KMnH	8.73(2)	-30.9(7)	2.00	5.91	16.0

after annealing at high temperatures confirm this conclusion. The TGA results also confirm the stoichiometry of the samples. If one compares the TGA results for the K samples, it appears that the thermal stability increases from Mn to Co and Ni. For a given transition metal, it is similar for Na and K compounds (Figure S8).

Infrared Spectroscopy. Comparison of the infrared spectra (Figure S9) of **KCoH** and **KCoD** allows one to distinguish between OH(D) and SeO_4 vibration bands. The shift between OH and OD stretching vibration bands at 3444 and 2498 cm^{-1}, 0.725, agrees with the calculated ratio of $(18/(17 \times 2))^{1/2} = 0.728$.[27,28] Both bands are very broad as expected for groups involved in hydrogen bonds. The residual band of O−H type in the **KCoD** results from incomplete substitution of D for H. The bending mode of the water molecule is evidenced at 1622 cm^{-1} for **KCoH** and 1190 cm^{-1} for **KCoD**. The out of plane deformation vibrations γ(OH) around 1170 and 722 cm^{-1} are shifted to 850 and 550 cm^{-1} for γ(OD), the first one being masked by the SeO_4 bands. On the other hand, the γ(OH) band ∼750 cm^{-1} corresponding to the γ(OD) band observed at 616 cm^{-1} falls in the SeO_4 band

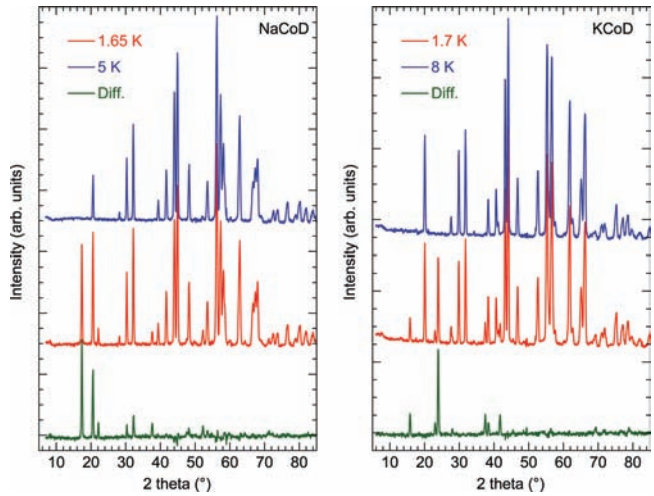

Figure 5. Neutron powder diffraction patterns recorded below (blue) and above (red) T_N and the difference (green) for **NaCoD** (left and Figure S10) and **KCoD** (right) on G4.1 diffractometer, λ =2.4266 Å.

region. Three sharp bands at 945, 854, and 812 cm^{-1}, not shifted from H to D, are attributed to vibrations of the SeO_4 group. According to Nakamoto, the ν_1 and ν_3 bands are observed at ∼875 cm^{-1} and 833 cm^{-1}, respectively. ν_1 is not IR active for a regular tetrahedron but becomes active for a distorted one. The distortion also explains the splitting of the ν_3 vibration band. The bands at 469 cm^{-1} could be attributed either to Co−O or $\nu_4(SeO_4)$ vibrations. As this band shifts according to the nature of the transition metal, the first

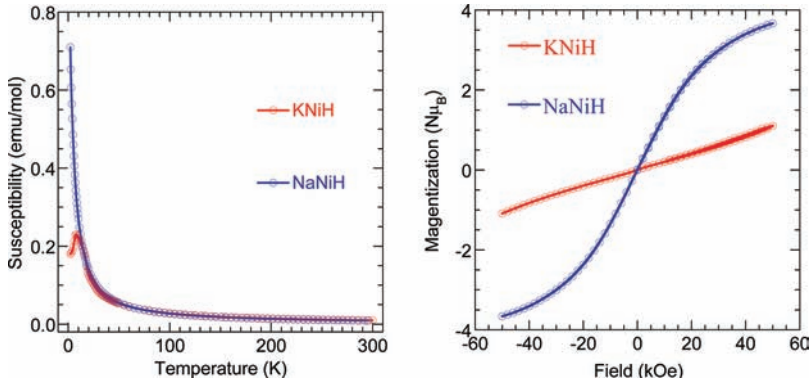

Figure 4. Magnetic susceptibility (left) and isothermal magnetization at 2 K (right) for **NaNiH** and **KNiH**.

dx.doi.org/10.1021/ic202273e | Inorg. Chem. 2012, 51, 1953−1962

Table 5. Irreducible Representations for NaCoD[a]

IR	moment	Co11 (1/4, 1/4, 0)	Co12 (3/4, 1/4, 0)	Co13 (3/4, 3/4, 0)	Co14 (1/4,3/4, 0)
Γ_2	M_x, M_y, M_z	+ + +	− + −	− − −	+ − +
Γ_4	M_x, M_y, M_z	+ + +	+ − +	− − −	− + −

[a]For **KCoD** the positions of the cobalt atoms (Co15−Co18) in the second cell are related to those of Co11−Co14 by (0, 0, 1/2) and have the respective IR.

Table 6. Components of the Magnetic Moment of Cobalt Atoms for NaCoD at 1.65 K

atom	M_x (μ_B)	M_y (μ_B)	M_z (μ_B)	M_{total} (μ_B)
Co11	0	2.51(2)	−1.29(4)	2.83(3)
Co12	0	−2.51(2)	−1.29(4)	2.83(3)
Co13	0	−2.51(2)	1.29(4)	2.83(3)
Co14	0	2.51(2)	1.29(4)	2.83(3)

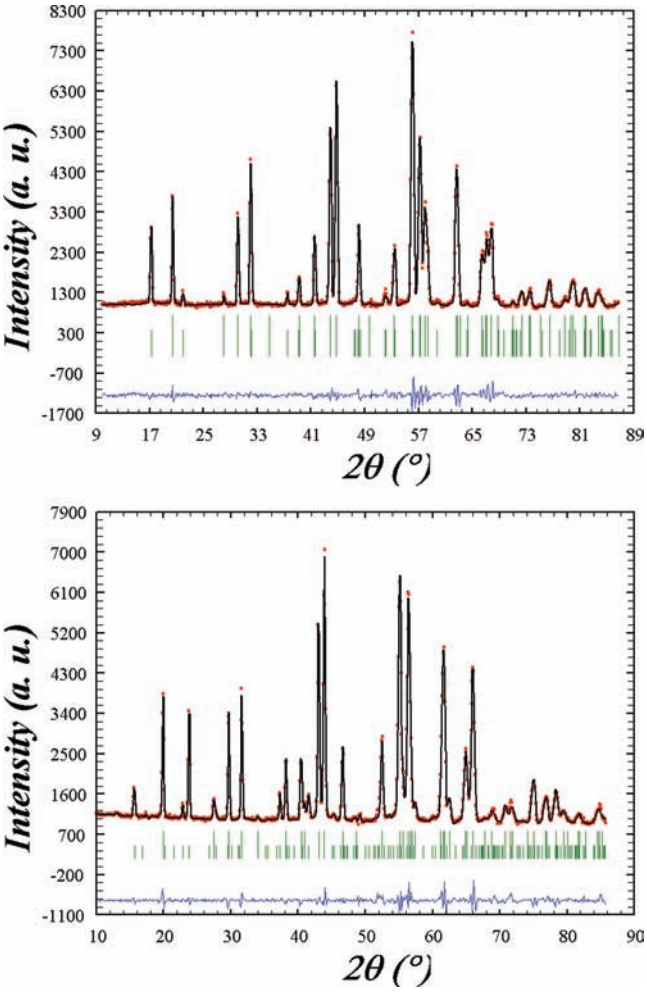

Figure 6. Observed (red) and calculated (black) profiles of **NaCoD** (top) at 1.65 K and **KCoD** (bottom) at 1.7 K using λ = 2.4266 Å with position of the Bragg lines, nuclear, LRO, SRO (green), and difference between observed and calculated profiles (blue).

attribution is more probable and its position does not vary from Na to K.

Magnetic Properties. Figure 3 presents the thermal evolution of the DC susceptibility for **NaCoH** and **KCoH**. In the paramagnetic region above 100 K, the susceptibility follows a Curie−Weiss law, $\chi = C/(T - \theta)$ with C = 6.12(1) and 5.97(1) emu K/mol and θ = −15.5(3) and −26.1(6) K for

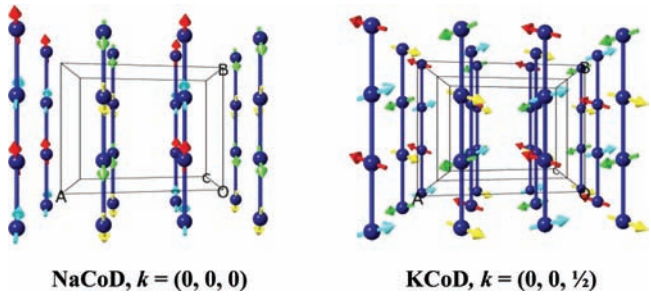

Figure 7. Magnetic structures of **NaCoD** and **KCoD**: Co11 (red), Co12 (green), Co13 (yellow), and Co14 (cyan).

NaCoH and **KCoH**, respectively. The negative value of the Weiss constant is related to antiferromagnetic interactions between near neighbor cobalt atoms. From the Curie constant, we can calculate the effective moments $\mu_{eff} = (8C)^{1/2}$ = 4.95 and 4.89 μ_B and the Landé factor $g = (8C/S(S + 1))^{1/2}$ = 2.55 and 2.52.[29] The effective moment is high compared to the expected value of 3.87 μ_B if only the spin contribution is considered. The difference is related to orbital contribution.

At low temperatures, the magnetic susceptibility defines a sharp peak in each case with its maximum at 3.5 K for **NaCoH** and 5.9 K for **KCoH**. Such behavior can be related to a transition toward antiferromagnetic ordering with T_N = 3.5 and 5.9 K, respectively. This conclusion is confirmed by the AC susceptibilities that exhibit a peak in their real component but no anomaly in the corresponding imaginary one.

The isothermal field dependence of the magnetization of the two compounds is shown in Figure 3b. Increasing the applied field promotes first a linear increase of the magnetization followed by a change of the slope at around 12 kOe for **NaCoH** then tending toward saturation at higher applied field. The anomaly at 12 kOe may be considered as a metamagnetic behavior.[30] The magnetization at 50 kOe is 4.65 μ_B, a value close to 4.3 μ_B being expected from parallel alignment of the moments of the cobalt atoms taking into account values of S_{eff} = 1/2 and $\langle g \rangle$ = 13/3 at low temperature for Co^{2+}. For **KCoH**, magnetization evolution is linear up to around 25 kOe then deviates from linearity. However, it is not possible to conclude whether the behavior is similar to the one observed for **NaCoH**, due to the limitation of the applied field.

NaNiH and **KNiH** behave as paramagnets above 100 K with the parameters given in Table 4. However, **NaNiH** exhibits a weak ferromagnetic interaction between nearest neighbor nickel atoms while **KNiH** shows a larger antiferromagnetic interaction (Figure 4). Furthermore, **NaNiH** does not show any long-range magnetic ordering while **KNiH** shows a downturn at 8.5 K, suggesting an antiferromagnetic ordering. The difference in ground states is also demonstrated in the isothermal magnetization where **NaNiH** displays a Brillouin type field dependence while **KNiH** shows an almost linear dependence without reaching saturation.

dx.doi.org/10.1021/ic202273e | Inorg. Chem. 2012, 51, 1953−1962

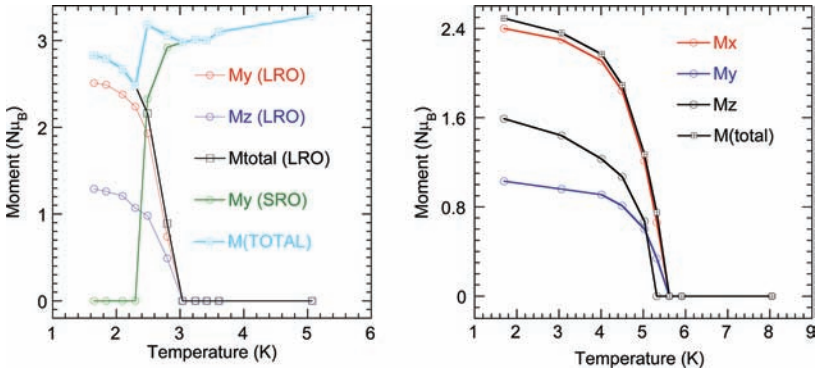

Figure 8. Temperature dependence of the components of the magnetic moments for (a) **NaCoD** with components of LRO and SRO structures and their sum as $M_{LRO+SRO} = (M_{LRO}^2 + M_{SRO}^2)^{1/2}$ and (b) the LRO of **KCoD**.

Table 7. Atomic Positions and Magnetic Moments from Data at 1.7 K for KCoD

atom	*x/a, y/b, z/c*	M_x (μ_B)	M_y (μ_B)	M_z (μ_B)	M (μ_B)
Co11	1/4, 1/4, 0	2.40(3)	1.03(3)	1.59(8)	2.49(3)
Co12	3/4, 1/4, 0	2.40(3)	−1.03(3)	1.59(8)	2.49(3)
Co13	3/4, 3/4, 0	−2.40(3)	−1.03(3)	−1.59(8)	2.49(3)
Co14	1/4, 3/4, 0	−2.40(3)	1.03(3)	−1.59(8)	2.49(3)
Co15	1/4, 1/4, 1/2	−2.40(3)	−1.03(3)	−1.59(8)	2.49(3)
Co16	3/4, 1/4, 1/2	−2.40(3)	1.03(3)	−1.59(8)	2.49(3)
Co17	3/4, 3/4, 1/2	2.40(3)	1.03(3)	1.59(8)	2.49(3)
Co18	1/4, 3/4, 1/2	2.40(3)	−1.03(3)	1.59(8)	2.49(3)

KMnH displays antiferromagnetic interaction and shows a Néel transition at 16 K. Table 4 summarizes the magnetic properties.

Magnetic Structures. All the Bragg reflections in the neutron diffraction pattern of **NaCoD** at 5 K were indexed in the Natrochalcite monoclinic *C*2/*m* space group, a = 8.9300(4) Å, b = 6.3631(2) Å, c = 7.5369(3) Å, and β = 115.083(2)°. The atomic positions were refined to final reliability factors R_B = 1.09, R_F = 1.39, R_p = 10.5, R_{wp} = 9.13. and R_{exp} = 4.01. The results confirm there is no change of the nuclear structure as a function of temperature except for a small contraction. The comparison of the neutron diffraction patterns recorded at 1.65 and 5 K (Figure 5) reveals the appearance of numerous new lines at 1.65 K and an increase of some of those observed at 5 K. Both contributions are of magnetic origin, with the appearance of the new ones being characteristic of antiferromagnetic ordering. All new lines can be indexed with the unit cell parameters of the natrochalcite structure and correspond to lines (100), (010), (−102), (−302), (102), (−122), normally forbidden for space group *C*2/*m*, i.e., lines with $h + k = 2n + 1$ and define a propagation vector k = (0, 0, 0). Moreover, an increase of the background as successive bumps, the more visible with its maximum around 2θ = 17°, is evidenced on patterns recorded above 2.5 K and is related to the presence of a short-range ordered structure (SRO, see Figure S10) whereas the sharp lines are due to long-range order magnetic structure (LRO).

The LRO magnetic structure has been determined using the irreducible representations (Table 5) calculated using the Basireps program according to Bertaut's group theory.[31,32] Table 6 summarizes the corresponding results, while Figure 6 shows the fitted neutron powder diffraction profile and Figure 7 shows the magnetic structure. Only Γ_4 can reproduce the observed magnetic Bragg reflections.

In this magnetic structure, the moments lie within the *bc* plane, as expected since the strongest magnetic Bragg reflection is the (100), with 4 sublattices of cobalt atoms as shown (different colors in Figure 7). The cobalt chains are ferromagnetically coupled with M_y = 2.51(2) μ_B and M_z = 1.29(4) μ_B, the resultant moment making an angle of 27° with the *b*-axis. Its value, 2.83(3) μ_B, is a bit smaller than the value currently observed for cobalt atoms, 3−3.3 μ_B. However, the fact that the measuring temperature is close to T_N could explain the observed value. Inside the layers containing the cobalt chains connected to each other by D_3O_2 and SeO_4 groups, the magnetic moments of two adjacent chains are canted in opposite directions, thus canceling each other. On the other hand, two successive layers adopt the same orientation.

To take into account the magnetic contribution from the bumps observed for $T \geq 2.5$ K, a second magnetic structure has been refined simultaneously, with the same model as for the LRO structure. Table S6 and Figure 8 show the results obtained for the refinement of data recorded at different temperatures. The evolution of the components has the typical shape for this kind of curve. The high value of $M_{LRO+SRO}$ at T = 2.5 K is related to the concomitant presence of both magnetic structures with a lower precision of their parameters.

Using the same procedure as for **NaCoD**, we find that the difference pattern for **KCoD** (8 and 1.7 K) is quite different from that of **NaCoD**; all the magnetic peaks correspond to a different set of Bragg reflections (Figure 5). These peaks can be indexed using a propagation vector k = (0, 0, 1/2), that is a doubling of the nuclear c parameter for the magnetic cell. The irreducible representation Γ_4 allows one to find the correct structural model that gives a good agreement between observed and calculated magnetic lines. Table 7 gives the components of the magnetic moments and Figures 6 and 7 show the fitted neutron powder diffraction profiles and the magnetic structure.

KCoD exhibits an antiferromagnetic structure consisting of four sublattices as observed for **NaCoD** but with magnetic moment components along the three crystallographic axes. It can be noticed that the ratio $M_i/\sigma(M_i)$ is quite different for all three components: 80, 34, and 20 for *a*, *b*, and *c*-axis, respectively. Within the cobalt chains, the major component of the coupling between nearest neighbor moments is AF along the [101] direction with a ferromagnetic component along the *b*-axis. Moments on adjacent chains in the *bc*-plane are aligned in the same direction giving an overall canted moment along the *b*-axis. Those on the adjacent layers along the *a*-axis have the same components along the *ac*-plane but with the canting pointing in the opposite direction along the *b*-axis. The final

dx.doi.org/10.1021/ic202273e | *Inorg. Chem.* 2012, 51, 1953−1962

result is a fully compensated antiferromagnet. Refinements of the data recorded at higher temperatures (Table S7 and Figure 8) reveal that the same magnetic structure is valid up to T_N. All components decrease up to 5.3 K, the M_z component being zero at this temperature and T_N between 5.3 and 5.6 K, in agreement with the susceptibility measurements, T_N = 5.9 K.

4. CONCLUSION

Five basic selenates, $AM_2(H_3O_2)(SeO_4)_2$, exhibiting the natrochalcite-type structure have been obtained by hydrothermal technique showing a tendency for higher stability when the size ratio of M to A is small. For example, the synthesis of the salt with the smaller A (Na) and the largest M (Mn), **NaMnH**, has not been successful. All the compounds but $NaNi_2(H_3O_2)(SeO_4)_2$ order antiferromagnetically with an upturn in magnetization in all cases at higher field suggesting either metamagnetism or spin-flop. The magnetic structures of **NaCoD** and **KCoD** are different from each other: the first one with ferromagnetic order within the edge-sharing cobalt chains, the second one with AF order within the chains. In relation to previously reported magnetic structures of this family of salts, this result appears to be related to the propagation vector, ferromagnetic coupling for k = (0,0,0) and antiferromagnetic coupling for $k \neq$ (0,0,0) which is verified for the seven magnetic structures known up to now for natrochalcite compounds. All seven known magnetic structures are surprisingly different from each other.

■ ASSOCIATED CONTENT

Supporting Information

X-ray crystallographic information file in CIF format; photo of the crystals; DT-TGA in air; infrared spectra; LeBail pattern matching fits of PXRD; susceptibility measured on cooling in different magnetic fields. This material is available free of charge via the Internet at http://pubs.acs.org.

■ AUTHOR INFORMATION

Corresponding Author

*E-mail: vilminot@ipcms.u-strasbg.fr. Tel: 00 33 3 88 10 71 28 (S.V.). E-mail: kurmoo@unistra.fr. Tel: 00 33 3 68 85 12 31 (M.K.).

■ ACKNOWLEDGMENTS

This work was supported by the CNRS (France), CEA (France), and the Université de Strasbourg (France). W.M. thanks the Université SFax (Tunisia) for a fellowship.

■ REFERENCES

(1) (a) Harrison, R. J. Magnetic properties of rocks and minerals. In *Treatise on Geophysics*; Elsevier: Amsterdam, 2008, *2*, 579. (b) *Physics meet Mineralogy*; Aoki, H, Syono, Y., Hemley, R. J., Eds.; Cambridge University Press: Cambridge, 2000.

(2) Cornell, R. M.; Schwertmann, U. *The Iron Oxides, Structure, Properties, Reactions, Occurrence and Uses*; VCH Publishers: Weinheim, Germany, 1996.

(3) (a) Schieber, M. M. *Experimental Magnetochemistry*; North-Holland Publishing Company: Amsterdam, 1967. (b) Goodenough, J. B. *Magnetism and the Chemical Bond*; John Wiley and Sons: New York, 1963. (c) Morrish, A. H. *The Physical Principles of Magnetism*; R.E. Krieger: Huntington, NY, 1980. (d) De Jongh, L. J., Ed. *Magnetic Properties of Layered Transition Metal Compounds*; Kluwer Academic Publishers: Dordrecht/Boston, MA, 1990.

(4) (a) *Neutron Diffraction*; Bacon, G. E., Clarendon Press: Oxford, 1962. (b) Blundell, S. J. *Magnetism in Condensed Matter*; Oxford, University Press: Oxford, 2001.

(5) (a) Harrison, A. *J. Phys: Condens. Matter* **2004**, *16*, S553. (b) Nocera, D. G.; Bartlett, B. M.; Grohol, D.; Papoutsakis, D.; Shores, M. P. *Chem.—Eur. J.* **2004**, *10*, 3850. (c) Wills, A. S. *Phys. Rev. B.* **2001**, *63*, 064430. (d) Shores, M. P.; Nytko, E. A.; Bartlett, B. M.; Nocera, D. G. *J. Am. Chem. Soc.* **2005**, *127*, 13462. (e) Behara, J. N.; Rao, C. N. R. *Can. J. Chem.* **2005**, *83*, 668–673. (f) Behara, J. N.; Rao, C. N. R. *Dalton Trans.* **2007**, 668. (g) Grohol, D.; Huang, Q.; Toby, B. H.; Lynn, J. W.; Young S. Lee, Y. S.; Nocera, D. G. *Phys. Rev. B* **2003**, *68*, 094404.

(6) Long, G. J.; Longworth, G.; Battle, P.; Cheetham, A. K.; Thundathil, R. V.; Beveridge, D. *Inorg. Chem.* **1979**, *18*, 624.

(7) Vilminot, S.; André, G.; Bourée-Vigneron, F.; Richard-Plouet, M.; Kurmoo, M. *Inorg. Chem.* **2007**, *46*, 10079.

(8) Vilminot, S.; Richard-Plouet, M.; André, G.; Swierczynski, D.; Bourée-Vigneron, F.; Kurmoo, M. *Dalton Trans.* **2006**, 1455.

(9) (a) Shores, M. P.; Bartlett, B. M.; Nocera, D. G. *J. Am. Chem. Soc.* **2005**, *127*, 17986. (b) Vilminot, S.; André, G.; Richard-Plouet, M.; Bourée-Vigneron, F.; Kurmoo, M. *Inorg. Chem.* **2006**, *45*, 10938.

(10) (a) Vilminot, S.; Richard-Plouet, M.; André, G.; Swierczynski, D.; Bourée-Vigneron, F.; Kurmoo, M. *Inorg. Chem.* **2003**, *42*, 6859. (b) Ben Salah, M.; Vilminot, S.; André, G.; Richard-Plouet, M.; Bourée-Vigneron, F.; Mhiri, T.; Kurmoo, M. *Chem.—Eur. J.* **2004**, *10*, 2048. (c) Ben Salah, M.; Vilminot, S.; André, G.; Bourée-Vigneron, F.; Richard-Plouet, M.; Mhiri, T.; Kurmoo, M. *Chem. Mater.* **2005**, *17*, 2612.

(11) Vilminot, S.; Baker, P. J.; Blundell, S. J.; Sugano, T.; Andre, G.; Kurmoo, M. *Chem. Mater.* **2010**, *22*, 4090.

(12) Ben Salah, M.; Vilminot, S.; Richard-Plouet, M.; André, G.; Mhiri, T.; Kurmoo, M. *Chem. Commun.* **2004**, 2548. (b) Ben Salah, M.; Vilminot, S.; André, G.; Richard-Plouet, M.; Mhiri, T.; Takagi, S.; Kurmoo, M. *J. Am. Chem. Soc.* **2006**, *128*, 7972. (c) Maalej, W.; Vilminot, S.; Andre, G.; Kurmoo, M. *Inorg. Chem.* **2010**, *49*, 3019.

(13) Takeda, S.; Watanabe, A.; Maruta, G.; Takasuke Matsuo, T. *Mol. Cryst. Liq. Cryst.* **2002**, *376*, 443.

(14) (a) Vilminot, S.; André, G.; Bourée-Vigneron, F.; Baker, P. J.; Blundell, S. J.; Kurmoo, M. *J. Am. Chem. Soc.* **2008**, *130*, 13490. (b) Maalej, W.; Vilminot, S.; André, G.; Damay, F.; Elaoud, Z.; Mhiri, T.; Kurmoo, M. *Inorg. Chem.* **2011**, *50*, 3286. (c) Maalej, W.; Vilminot, S.; André, Elaoud, Z.; Mhiri, T.; Kurmoo, M. *Inorg. Chem.* **2011**, *50*, 9191.

(15) (a) http://www.mindat.org/min-2853.html. (b) Palache, C. *Am. J. Sci.* **1939**, *237*, 451. (c) Palache, C.; Berman, H.; Frondel, C. *The System of Mineralogy of James Dwight Dana and Edward Salisbury Dana, Yale University*, 7th ed.; John Wiley and Sons, Inc.: New York, 1951; Vol. *II*, p1837.

(16) (a) Rumanova, I. M.; Volodina, G. F. *Doklady Acad. Nauk SSSR* **1958**, *123*, 78. in Russian (b) Pezerat, H. *CR Acad. Sci. Paris* **1965**, *261*, 5490. (c) Pezerat, H.; Mantin, I.; Kovacevic, S. *C.R. Hebd. Séances Acad. Sci., Ser. C* **1966**, *263*, 60. (d) Pezerat, H. *Bull. Soc. Fr. Minéral. Cristallogr.* **1967**, *90*, 549. (e) Pezerat, H. *C.R. Hebd. Séances Acad. Sci., Ser. C* **1967**, *265*, 368. (f) Cord, P.-P.; Courtine, P.; Pannetier, G. *C. R. Acad. Sci. Paris, Serie C* **1970**, *270*, 946. (g) Tardy, M.; Bregeault, J.-M. *Bull. Soc. Chim. France* **1974**, 1866. (h) Clearfield, A.; Sims, M. 1.; Gopal, R. *Inorg. Chem.* **1976**, *15*, 335. (i) Clearfield, A.; Sims, M. J.; Gopal, R. *Inorg. Chem.* **1985**, *24*, 4606. (j) Clearfield, A.; Moini, A.; Rudolf, P. R. *Inorg. Chem.* **1985**, *24*, 4606. (k) Moini, A.; Clearfield, A.; Jorgensen, J. D. *Acta Crystallogr.* **1986**, *C42*, 1667. (l) Palacio, L. A.; Echavarra, A.; Saldarriaga, C. *Int. J. Inorg. Mater.* **2001**, *3*, 367. (m) Jang, M.; Weakley, T. J. R.; Doxsee, K. M. *Chem. Mater.* **2001**, *13*, 519. (n) Chu, D.-Q.; Pan, C.-L.; Duan, L.-M.; Xu, J.-Q.; Wang, L.-M.; Yu, J.-H.; Wang, T.-G. *Inorg. Chem. Commun.* **2002**, *5*, 989.

(17) (a) Giester, G. *Z. Kristallogr.* **1989**, *187*, 239. (b) Giester, G.; Zemann, J. *Z. Kristallogr.* **1987**, *179*, 431.

(18) (a) Krickl, R.; Wildner, M. *Eur. J. Mineral.* **2009**, *21*, 65. (b) Krickl, R.; Wildner, M. *Eur. J. Mineral.* **2007**, *19*, 805.

(19) (a) Chevrier, G.; Giester, G.; Jarosch, D.; Zemann, J. *Acta Crystallogr.* **1990**, *C46*, 175. (b) Chevrier, G.; Giester, G.; Zemann, J. *Z. Kristallogr.* **1993**, *206*, 7.
(20) Maalej, W. PhD Thesis, Université de Strasbourg, 2011.
(21) Sheldrick, G. M. 97-2 ed., University of Göttingen, Germany, 1997.
(22) Rodriguez-Carvajal, J. *FULLPROF: Rietveld, Profile Matching and Integrated Intensity Refinement of X-Ray and/or Neutron Data*, 3.5d Version; Leon-Brillouin Laboratory/CEA Saclay: France, 2005.
(23) Boultif, A.; Louer, D. *J. Appl. Crystallogr.* **2004**, *37*, 724.
(24) (a) Shannon, R. D.; Prewitt, C. T. *Acta Crystallogr.* **1969**, *B25*, 925. (b) Shannon, R. D.; Prewitt, C. T. *Acta Crystallogr.* **1970**, *B26*, 1046. (c) Shannon, R. D. *Acta Crystallogr.* **1976**, *A32*, 751.
(25) Brown, I. D.; Altermatt, D. *Acta Crystallogr.* **1985**, *B41*, 244.
(26) Steiner, T. *Angew. Chem., Int. Ed.* **2002**, *41*, 48.
(27) Nakamoto, K. *Infrared and Raman Spectra of Inorganic and Coordination Compounds*, 5th ed.; John Wiley & Sons: New York, 1997.
(28) Beran, A; Giester, G; Libowitzky, E. *Mineral. Petrol.* **1997**, *61*, 223.
(29) (a) Herpin, A. *Theorie du Magnétisme*; Presses Universitaire de France: Paris, 1968. (b) Mulay, L. N., Boudreaux, E., Eds.; *Theory of Molecular Paramagnetism*; Wiley: New York, 1976.
(30) Marvilliers, A.; Parsons, S.; Riviere, E.; Audiere, J.-P.; Kurmoo, M.; Mallah, T. *Eur. J. Inorg. Chem.* **2001**, *5*, 1287.
(31) Bertaut, E. F. *Acta Crystallogr., Sect. A* **1968**, *24*, 217.
(32) (a) KAREP– a program for calculating irreducible space group representations. Hovestreydt, E.; Aroyo, I.; Sattler, S.; Wondratschek, H. *J. Appl. Crystallogr.* **1992**, *25*, 544. (b) BASIREPS – a program for calculating non-normalized basis functions of the irreducible representations of the little group Gk for atom properties in a crystal. Rodriguez-Carvajal, J. Laboratoire Léon Brillouin (CEA(CNRS), CEA Saclay, Gif sur Yvette: France, 2004.